Robot Tactile Sensing

Gold Nanocomposites as Highly Sensitive Real-Time Optical Pressure Sensors

By Alessandro Massaro, Fabrizio Spano, Paolo Cazzato, Carola La Tegola, Roberto Cingolani, and Athanassia Athanassiou

In this article, we propose a new class of optical pressure sensors suitable for robot tactile sensing. These sensors are based on a tapered optical fiber (where optical signals travel) embedded onto a polydimethylsiloxane (PDMS)–gold nanocomposite material (GNM). By applying different pressure forces to the PDMS-based nanocomposite, we measure in real time the change of optical transmittivity due to the coupling between the GNM and tapered fiber region. The intensity reduction of the transmitted light intensity is correlated with the magnitude of the pressure force.

Sensory information from the human skin for feeling materials and determining their physical properties is provided by sensors in the skin. Presently, many researchers are attempting to apply the five senses to intelligent robot systems. In particular, many kinds of tactile sensors combining small force sensors have been introduced to intelligent robots. These tactile sensors, which are capable of detecting contact force, vibration, texture, and temperature, can be recognized as the next generation of information collection systems. Future applications of engineered tactile sensors include robotics in medicine for minimally invasive microsurgeries, military uses for dangerous and delicate tasks, and automation in industries. Some tactile sensors and small force sensors using microelectromechanical systems (MEMS) technology have been introduced. MEMS tactile sensing work has mainly focused on silicon-based sensors that use piezoresistive [1]–[3] or capacitive sensing [4]–[6]. These sensors have been realized with bulk and surface-micromachining methods. Polymer-based devices that use piezoelectric polymer films [7]–[9], such as polyvinylidene fluoride (PVDF) for sensing, have also been demonstrated. Although these sensors offer good spatial resolution due to the use of MEMS techniques, they still have problems with applications to practical systems. In particular, devices that

Digital Object Identifier 10.1109/MRA.2012.2184198

Date of publication: 29 February 2012

1070-9932/13/$31.00©2013IEEE

incorporate brittle sensing elements, such as silicone-based diaphragms or piezoresistors, are not reliable for robotic manipulation. Previous efforts have been hindered by rigid substrates, fragile sensing elements, and complex wiring.

Moreover, the polymeric solutions that can be found in literature for the fabrication of pressure sensor systems [10]–[14] require complex fabrication processes and postprocessing analysis. These drawbacks can be compensated for by using flexible optical fiber sensors and transducers. In addition, optical fiber sensors are immune to electromagnetic (EM) fields and can be easily multiplexed and integrated with small light emitting diode (LED) sources, thus providing a good alternative for the implementation of robotic tactile sensors [15]–[23]. Therefore, in this article we present a newly designed optical fiber force sensor based on the EM coupling effect. The prototype sensor is illustrated in Figure 1(a): a tapered multimode S_i fiber couples the EM field originating from a broad band-lamp source with a flexible polymer–GNM illustrated in Figure 1(b).

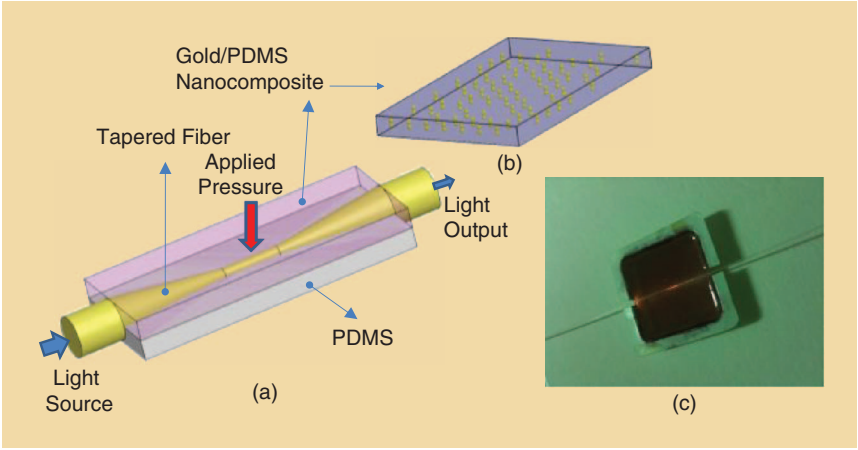

Figure 1. (a) Schematic configuration of the first prototype optical pressure sensor. (b) Model of the nanocomposite material with gold nanoparticles used for the light coupling. (c) Photo of the fabricated prototype sensor with light going out from the tapered fiber profile.

A PDMS polymer film was chosen for the proposed sensor because of its ability to generate gold nanoparticles starting from gold precursors [24], [25]. Moreover, PDMS presents good elastomeric properties that make it possible to obtain a real-time pressure sensor response. The sensor illustrated in Figure 1(c) is the optimized version obtained after previous preliminary studies, where the key parameter was the PDMS–gold controlled thickness. The half-diameter GNM thickness is chosen for two important reasons. The first reason is technological: accurate control of GNM deposition is actually difficult, which is why we decide to choose the fiber diameter as a reference level. The second reason is an economic one: the idea was to decrease the amount of gold quantity in the perspective of a possible industrial-oriented production. The first prototype is based on a nonintegrated cap of PDMS-Au material placed on a tapered fiber [26]. For this first prototype, we have observed a low sensitivity in the order of approximately 20 g. The choice of half-embedded fiber, as shown in Figure 1, is due to the possibility of allowing an optical integrated system to provide better mechanical stability and, finally, to perform higher sensitivity. The sensitivity can be optimized by increasing the effective refractive index near the coupling interface (interface between the tapered fiber and GNM). The increase of the coupling is due to the applied pressure.

Technological Aspects and Design

The technological aspects and the pressure application modalities of the proposed sensors are illustrated in detail in Figure 2. In particular, Figure 2(a)–(d) refer to the proposed prototype. The bottom half of the tapered fiber is embedded in a PDMS material to improve its mechanical stability. The PDMS is obtained by a classical/chemical procedure (a curing agent with a 1:10 weight ratio to base polymer is used). We control the deposition of PDMS by using the initial liquid state of the PDMS; hence, we added liquid PDMS to immerse only half-tapered fiber, as illustrated in Figure 2.

Sensory information from the human skin for feeling materials and determining their physical properties is provided by sensors in the skin.

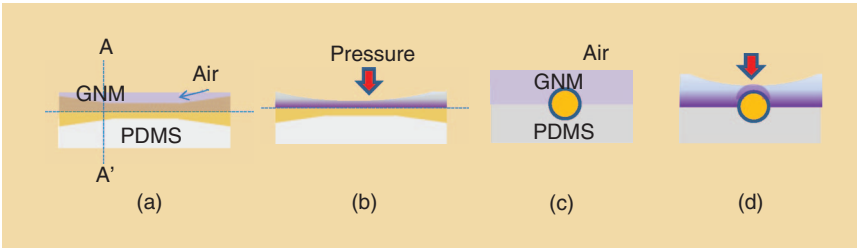

Figure 2. Technological aspects and pressure application modality of the proposed sensors. The tapered fiber is half embedded in PDMS and half in PDMS-Au material. Longitudinal section of the prototype (a) without and (b) with applied pressure. Cross section AA′ of the prototype (c) before and (d) after the application of pressure.

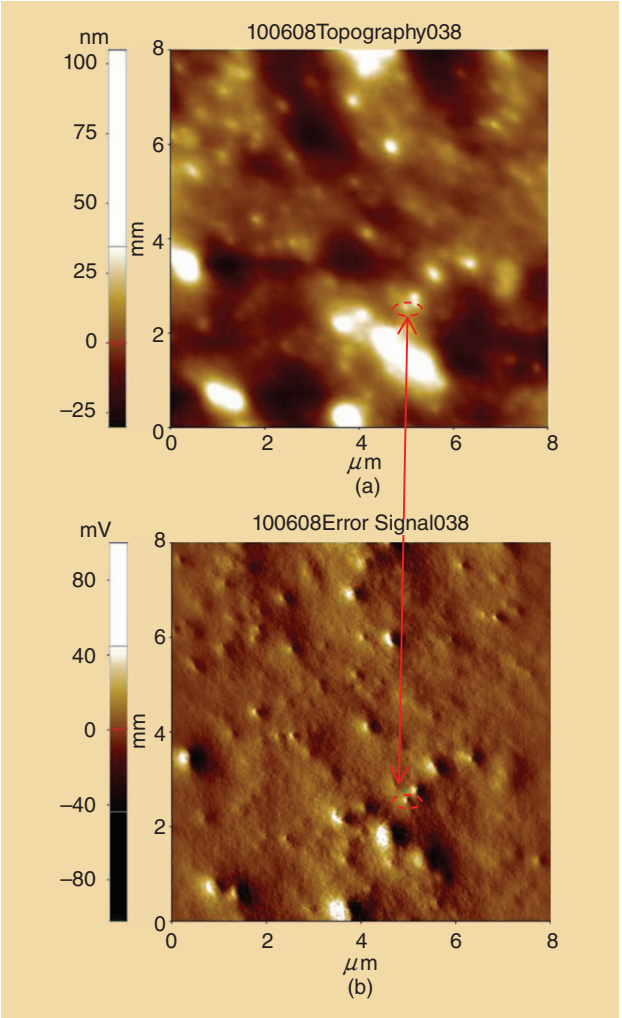

Figure 3. AFM images made on a cross section of PDMS GNM. (a) Topography and (b) error signal of the AFM image.

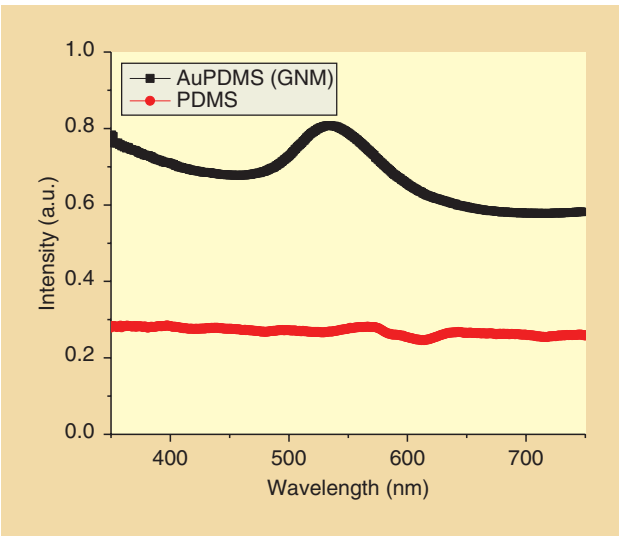

Figure 4. Experimental UV–visible spectra of the GNM sample used for the pressure sensor. This, with Figure 3, indicates the presence of gold micro/nanoparticles.

A period of two days is necessary to reach the solid/elastomeric state of the PDMS without heating. The prototype is obtained by depositing the GNM of a specific gold concentration. The tapered fiber is a coated silica/core silica multimode optical fiber (FG-365-LER Thorlabs fiber) tapered by a controlled system. The system makes it possible to uniformly pull the fiber by rotating it and simultaneously by burning the jacket and the cladding for some seconds (the number of seconds is related to the intensity and to the distance of the flame). This process improves a 1 cm of the total tapered profile with about 5 mm of central core region without cladding.

Figure 2(a) and (b) shows the longitudinal section of the prototype without and with the applied pressure force, respectively. The piece of GNM behaves as a cap and covers the remaining upper part of the tapered fiber. In this way, the contact interface becomes more efficient for the light coupling between the tapered fiber and GNM. Figure 2(c) and (d) illustrates the longitudinal section of the optimized prototype without and with the applied pressure force, respectively: the GNM deposition is controlled to perfectly cover the upper half of the tapered fiber, as indicated in the cross section of the core region of Figure 2(d). The optimized total thickness of the GNM layer was found to be equal with half diameter of the fiber. The main physical principle of the sensor is illustrated in Figure 2(d), where we can observe the importance of the contact boundary between the fiber and GNM after the application of the pressure: in this case, the gold nanoparticles near the contact surface increase the intensity of light coupling. Two days are adequate to transform the deposited liquid GNM into a solid elastomeric material. Because of the controlled GNM PDMS deposition, the contact interface increases the efficiency of the sensor since thewhole tapered region is totally embedded in GNM.

The atomic force microscopy (AFM) images of the cross section of the GNM (Figure 3) provide information about the dimensions of the nanofillers inside the PDMS nanocomposite material. A nonuniform nanoparticles dispersion is observed.

Previous studies demonstrate that the use of the PDMS polymer helps to generate gold nanoparticles by reducing the gold precursor [24]–[25]. In our study, we establish a high gold concentration that preserves the elastomeric properties of the GNM for real-time pressure detection. In this specific case, we use a chloroauric acid salt as a gold precursor in water solution [Mw(HAuCl4) = 339.785g/mol; [HAuCl4] = 0.01M] with a concentration of approximately 10% by weight. The presence of gold verified in Figure 3 is also proved in Figure 4, representing the experimental ultraviolet (UV)–visible spectra of the GNM sample used for the pressure sensor prototype; pure PDMS does not show any absorbance in the visible region, whereas Au-PDMS (GNM) has an absorbance centered at $\lambda \cong 530$ nm. The full characterization of the

formed gold nanoparticles will be addressed elsewhere.

Basic Physical Principle: EM Coupling by Applied Pressure and Experimental Observations

The gold nanoparticles formed in the PDMS material are expected to increase the effective refractive index of the PDMS and support EM coupling with the tapered region of the fiber since the transmitted light tends to preferentially propagate into regions with a high refractive index. As shown in Figure 5(a), the pressure applied to the GNM introduces a displacement of nanoparticles along its interface with the tapered fiber increasing the light scattering; the nanoparticles thus increase the coupling of light with the GNM, reducing the transmitted light intensity of the optical fiber.

Regarding the modifications of the optical properties of the GNM, the effect of nanoparticle displacements due to the applied pressure is to change the effective refractive index of GNM as a function of the gold concentration. In particular, we can model the gradual variation of the GNM effective refractive index, as illustrated in Figure 5(b), where the region with a higher refractive index is near the contact interface of the tapered fiber and the region with a lower effective refractive index is toward the pressure contact surface. This variation of the effective refractive index can be approximately estimated assuming spherical gold nanoparticles in the PDMS material. In this case, the effective dielectric function ε_{eff} for spherical gold particles having dielectric function ε_m, which varies with the optical working wavelengths [26], embedded in a medium ε_s is defined by [27]–[28] as

$$\mathcal{E}_{\text{eff}} = \mathcal{E}_s \frac{\mathcal{E}_m(1+2\phi)+2\mathcal{E}_s(1-\phi)}{\mathcal{E}_m(1-\phi)+\mathcal{E}_s(2+\phi)}, \qquad (1)$$

where ϕ indicates the gold concentration.

The displacement of the gold nanoparticles in PDMS due to a uniformly applied force are schematically indicated by the bidimensional (2-D) FEMsimulation of Figure 6(a): the particles that are on the top of the GNM microcell region tend to accumulate near the contact interface by increasing the effective dielectric function of ε_{eff} due to the increment of ϕ, as schematized in Figure 5(b). The exact distribution of the function ε_{eff} during the applied force is difficult to model. To explain the basic principles through an approximated model, we assume high gold concentration for the region with higher effective permittivity in contact with the tapered region and a reduction of ε_{eff} to a different extent. The 2-D FEM simulation of Figure 6(b) shows that the EM energy is confined to where the effective permittivity is higher (pressure effect) by reducing the transmitted light intensity at the output of the fiber. The parameters used in the FEM simulation are

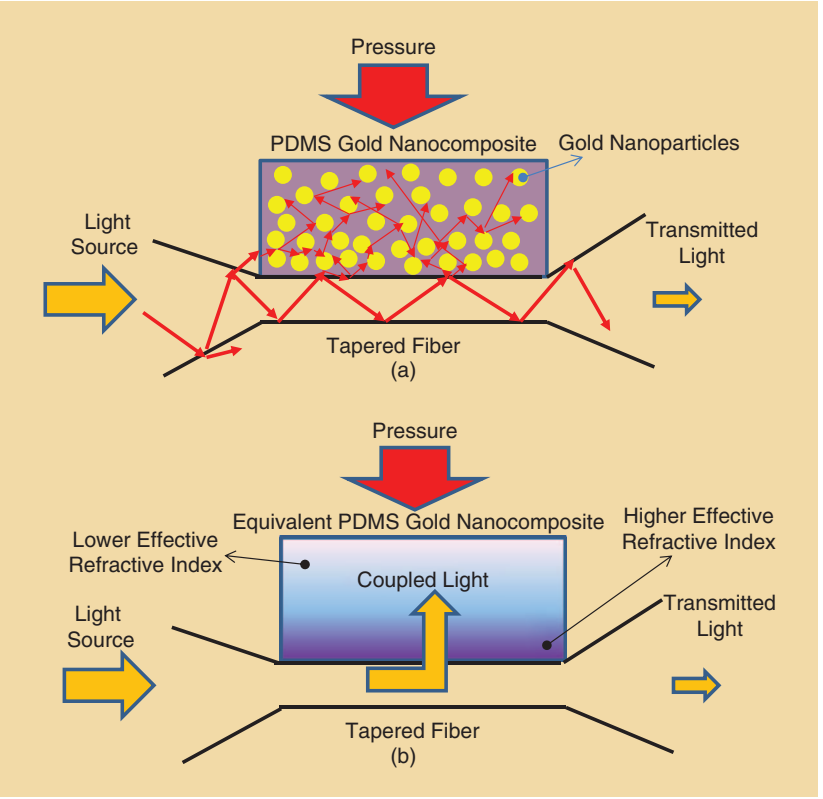

Figure 5. (a) Light coupling in GNM and light scattering process due to the gold micro/nanoparticles. (b) Equivalent nanocomposite material as a gradual variation of the effective refractive index.

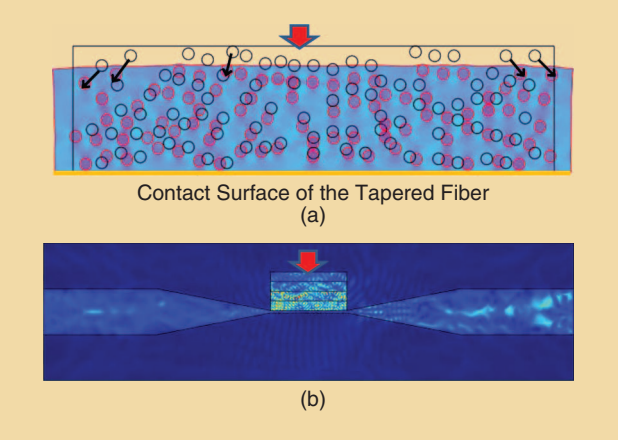

Figure 6. (a) 2-D mechanical FEM modeling of a GNM microcell: gold nanoparticle density correlated to the applied force. The simulated particles have a diameter of 120 nm. (b) 2-D FEM modeling: simulated modeling of Figure 5, where the results are obtained by reducing the value of the effective permittivity step by step by a factor two (corresponding to a theoretical reduction of gold concentration). The light coupling effect is strong in proximity of the tapered fiber interface.

Table 1. Parameters used in the FEM simulation.

Parameter	Description	Value
λ_0	Working wavelength	1.3 μm
$\varepsilon_{\text{fiber}}$	Relative dielectric permittivity of the core of the tapered fiber	3.17
ε_s	Relative dielectric permittivity of PDMS	2.25
ε_{eff}	Real part of the relative dielectric permittivity of the gold nanoparticle with $\phi = 0.5$ [first layer of GNM of Figure 5 (b)]	10
ρ_{gold}	Density of gold	19,300 kg/m^3
ρ_{PDMS}	Density of PDMS	970 kg/m^3
E_{gold}	Young's modulus of gold	70×10^9 Pa
E_{PDMS}	Young's modulus of PDMS	500×10^3 Pa
v_{gold}	Poisson's ratio of gold	0.44
v_{PDMS}	Poisson's ratio of PDMS	0.5

reported in Table 1. We have used a properly designed FEM tool oriented on micro-EM issues [29]. To highlight the importance of GNM for light coupling, we simulate and measure the coupling effect by considering PDMS and PDMS GNM, simply positioned on the tapered profile (without applied forces). Figure 7 shows the comparison between the transmitted optical intensities, taking into account the light

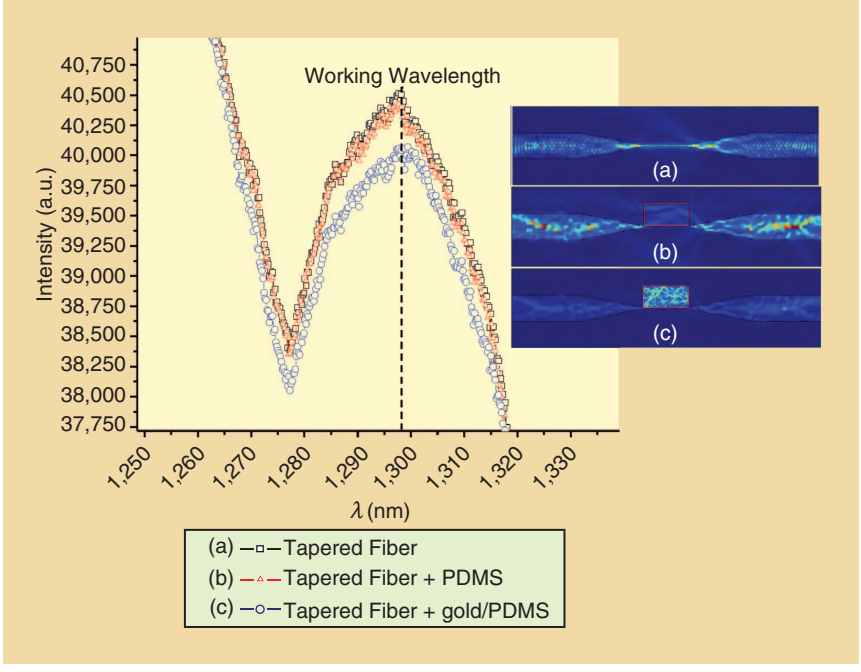

Figure 7. Experimental characterization of the light coupling without applied pressureforces: part of the transmittivity optical spectrum for (a) tapered fiber, (b) tapered fiber with PDMS material placed on the tapered region, and (c) tapered fiber with gold/PDMS material. Inset: 2-D FEM results. (a) FEM example of light coupling in an Si-tapered fiber, (b) small coupling effect by positioning a PDMS material on the tapered surface, and (c) high light coupling effect performed by placing it on the tapered region of the GNM. The working wavelength is $\lambda_0 = 1.298$ nm. The inset proves the experimental results reported in the figure.

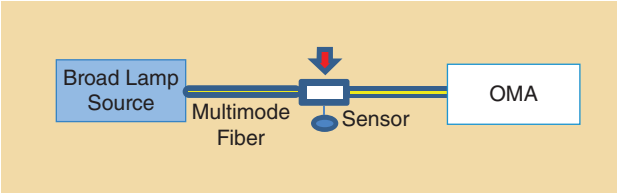

Figure 8. A schematic plot of the used experimental setup that includes a broad lamp source and an OMA.

transmitted in the tapered Si fiber [Figure 7(a)], the light transmitted and coupled for a fiber/PDMS system [Figure 7(b)], and the light transmitted and coupled for a fiber/GNM system [Figure 7(c)], respectively. A remarkable reduction of the transmitted light, due to coupling with GNM, is experimentally observed in the spectral range between 1,280 and 1,320 nm. Besides, no considerable variations are found in the same range by comparing the case of the tapered Si fiber and fiber/PDMS system. The same behavior of light intensity reduction is predicted by FEM simulations (see inset of Figure 7). Due to the multimodal propagation of light in the fiber, the variations of the transmitted light intensities are enhanced in specific frequency band regions. One of these regions is shown in Figure 7.

Measurements and Discussions

The measurements presented in Figure 7 and the ones of optical characterization of the proposed sensor upon pressure are performed using the experimental setup shown in Figure 8. An optical multichannel analyzer (OMA) is connected with the output of the multimode tapered fiber. The pressure sensor sample is fixed on a system that assures the mechanical stability during the application of the pressure forces. The input of the fiber is connected to a broad lamp source. We observe that the proposed technology is suitable for pressure sensors that can detect forces that are applied by different weights ranging from a few grams (0.01 N) to 200 (1.9 N) and 400 g (3.9 N). In each case, by applying different weights to the sensors a significant variation of the transmitted light intensity occurs. An example of real-time response is shown in Figure 9, where the optical response returns to the initial configuration after the measurements and the fast light transmittivity response is thus verified. We experimentally observe a quasi-simultaneous return to the initial spectrum as soon as we remove the weights (a response time less than 1 s is checked).

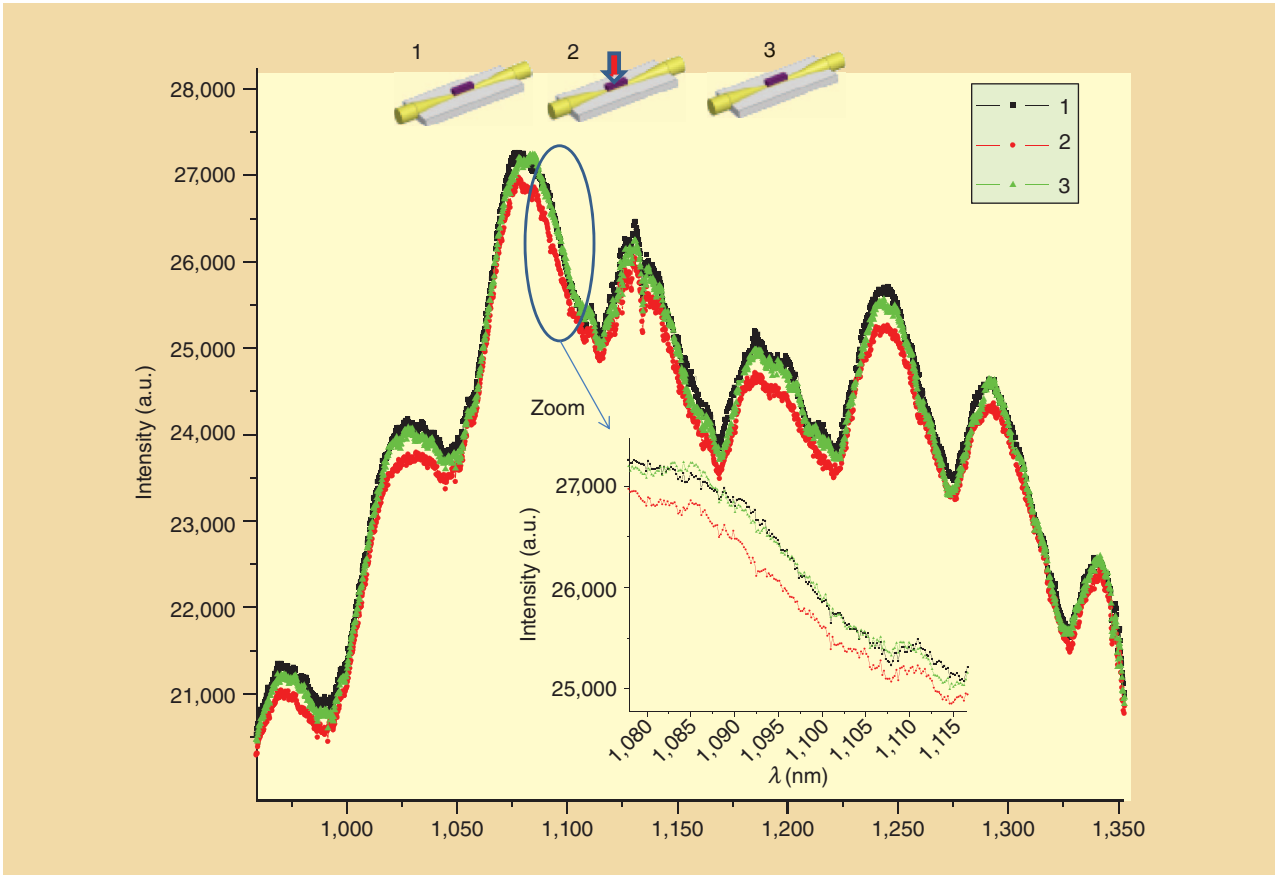

Figure 9. Real-time characterization of the pressure sensor by means of the transmittivity spectrum: Plot 1 represents the initial step (no forces are applied), plot 2 indicates the variation of the transmittivity response due to the applied weight of 118 g, and plot 3 is the transmittivity response immediately after the removing of the weight. Inset below: zoomed image of a part of a spectrum. The plots refer to a sensor able to detect high pressure forces.

The totally embedded configuration of the tapered fiber [Figure 2(c)] provides the best sensor sensitivity, compared to all the others we have tested. In fact, Figure 10 proves that the proposed sensor has the sensitivity to distinguish the pressure applied by a weight of only 5 g. For each plot of Figure 10, the average value of five measurements is

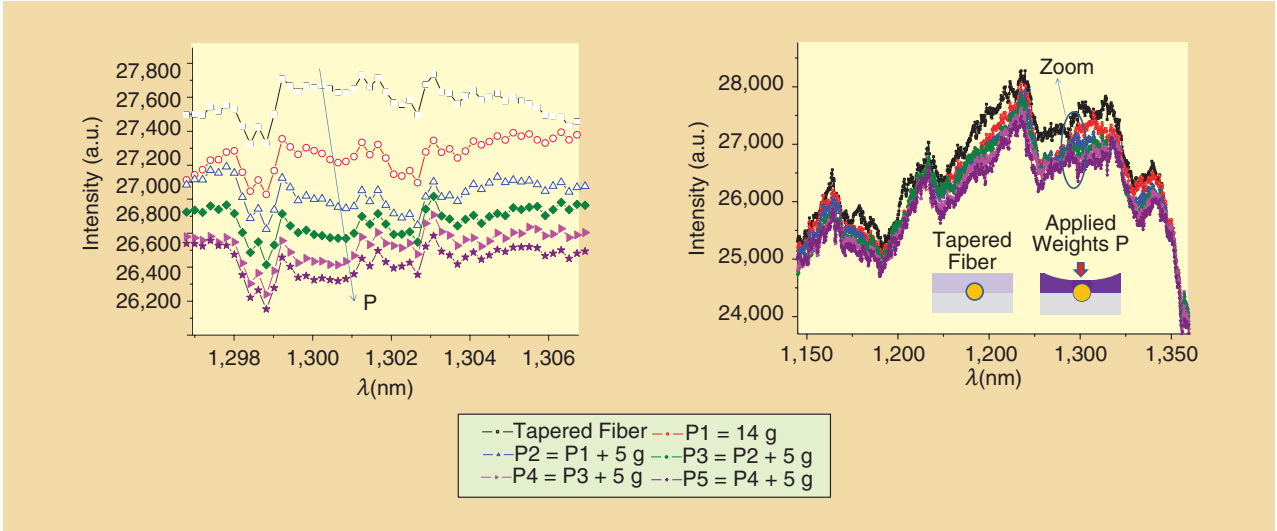

Figure 10. Experimental results of a part of the transmitted spectrum of the optimized device. Inset above: zoomed image of a spectrum region representing the optical losses following the applied pressures. Insets below: geometrical configurations illustrating the mechanical/optical effect of the applied weights.

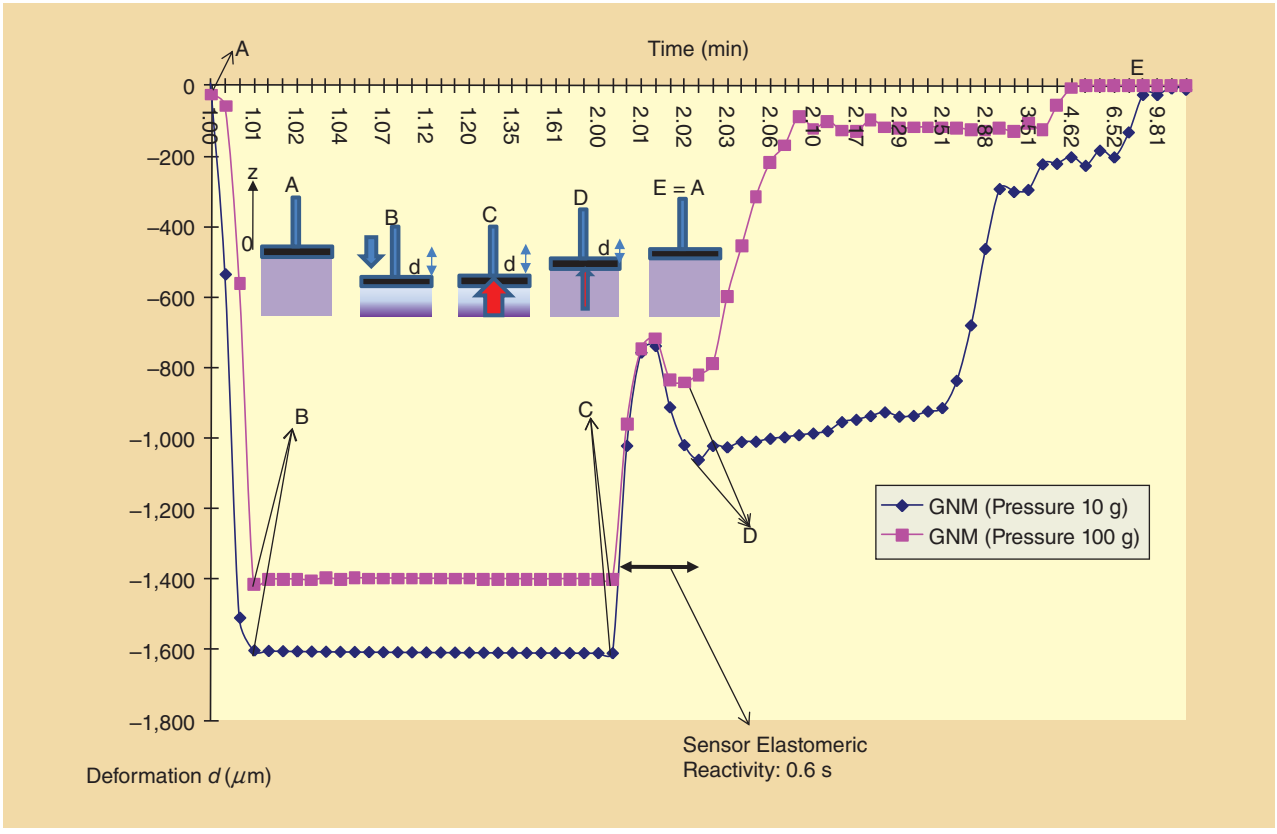

Figure 11. Experimental elastomeric deformation measurements of a GNM sample. Inset: mechanical evolutions of the elastomeric deformation type measurements according to the positions A–E reported in the plot.

considered. During the measurements of the prototype, we use a controlled system of weights that does not move the sensor during the experimental process and allows increasing of the pressure in steps applied by 5 g.

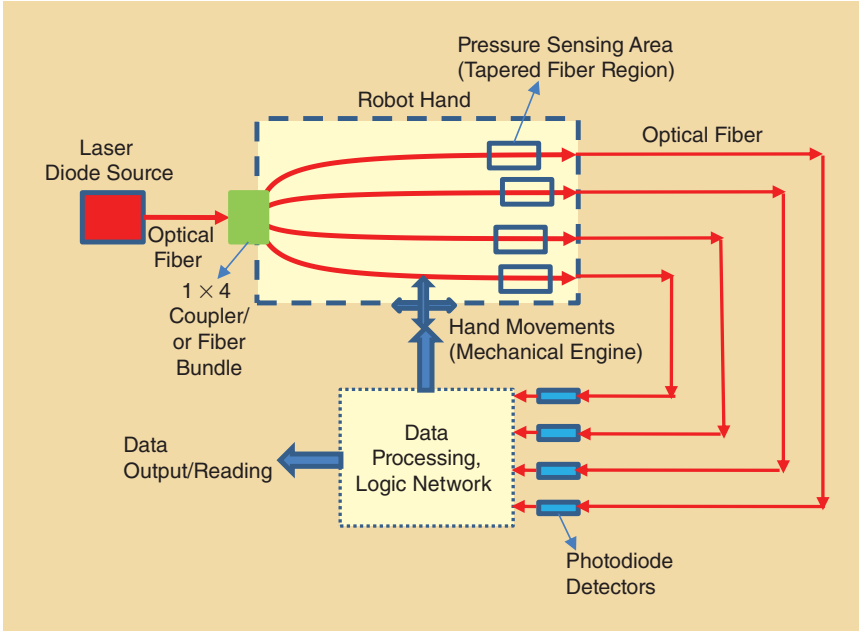

Figure 12. Functional diagram of the proposed sensor in a robotic system: a laser source (or a broad lamp source) is connected to a coupler or fiber bundle that splits the signalsinto different pressure sensors representing the robotic hand. Each sensor will transmit the signals to photo diodes that will convert the optic signal into an electrical one allowing signal processing and by properly designed electronic circuits.

The real-time behavior is further verified by measuring an elastomeric reactivity response time of 0.6 s, according to optical reactivity. The elastomeric sensor reactivity is performed by TA Instruments dynamical mechanical analyzer (DMA) Q800 machine. The measurement of elastomeric deformation, shown in Figure 11, provides information about the GNM elastomeric reaction time by applying pressure forces of 0.98 N (corresponding to about 100 g) and 0.098 N (corresponding to about 10 g). The elastomeric deformation indicates slow deformation of the used GNM measured under constant stress: the GNM sample (width = 4.77 mm, length = 14.96 mm, and thickness = 3.57 mm) deformation is monitored as a function of time. The GNM sample is then released to an unstressed state and its sample deformation recovery is monitored.

As illustrated in Figure 11, the reactivity of the sensor, in agreement with the optical measurements, is defined when the first recovery deformation occurs (interval of the time between states C and D).

Application: A Brief Introduction to Tactile Sensing for Robot Systems Architecture

The proposed sensor can be easily implemented in robotic tactile systems. By using small laser diode sources and small photodiode detectors, the pressure sensor requires small spaces and assures very fast detection responses. A possible schematic representation is illustrated in Figure 12, where an array of sensors indicates the fingers of a robotic hand. The sensor can be coupled to a little laser diode source by means of a coupler or fiber bundle. The signals coming from each sensitive sensor can be detected by photodiode detectors and can be processed by a logic network, providing by a controlled feedback system, commands about the possible movements of the sensors. The first prototype of the tactile finger robotic sensor is shown in Figure 13. In this prototype, a tapered fiber [see Figure 13(a)] passes inside a polyvinyl chloride (PVC) support representing the shape of a finger. To improve mechanical stability, the tapered profile is glued to the PVC support by means of Thorlabs epoxy glue for fiber optic connectors. The high sensitivity of pressure detection is performed by embedding all the PVC support in GNM. Figure 13(b) and (c) show the reported images of the robotic finger prototype. A possible experimental setup scheme for electrical measurements suitable for robotic systems and signal processing is illustrated in Figure 13(d), where a broad lamp is connected with the tapered fiber sensor, which transmits the signal to a photodetector that has the ability to convert the optical signal into an electrical one.

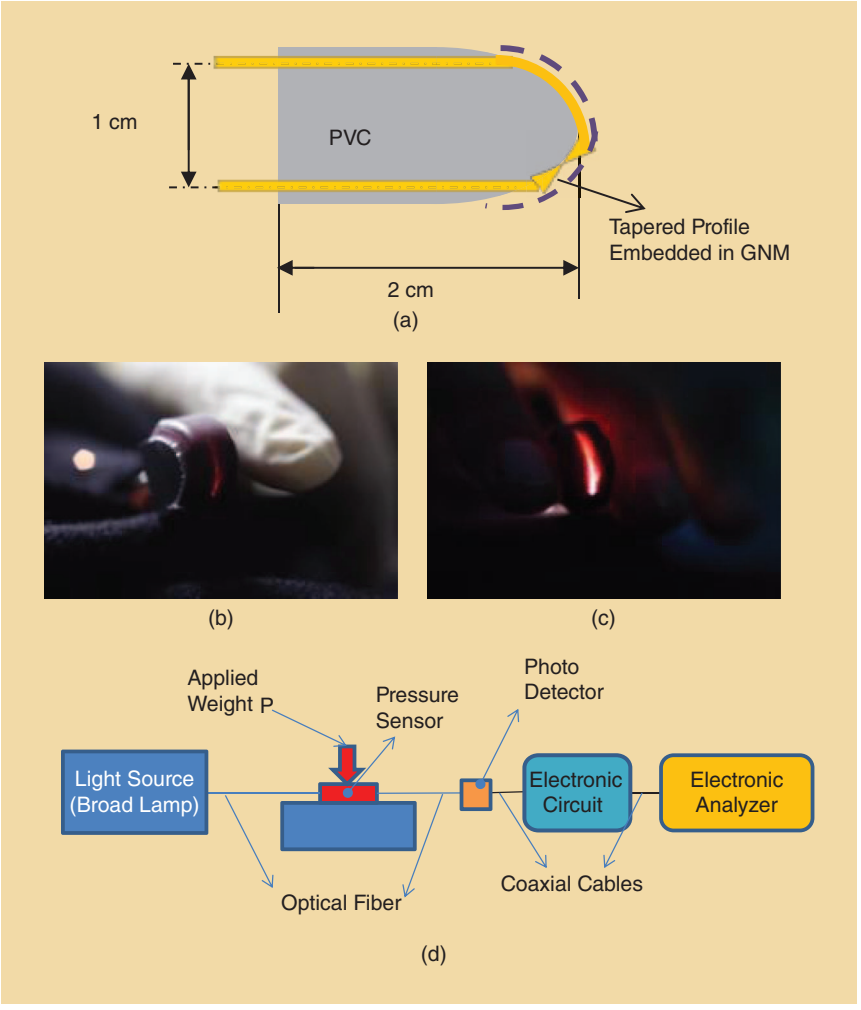

Figure 13. (a) Design of robotic finger by GNM. (b) and (c) Images of the light coupled inside the GNM: the light is emitted from the tapered profile and propagates inside the GNM (the light losses will increase as the pressure is applied to the finger). (d) A schematic diagram of the experimental setup suitable for robotic finger implementation.

Conclusions

In this article, we presented a new concept of an optical tactile sensor based on PDMS–GNM. The sensor is designed and optimized by means of experimental optical and preliminary mechanical characterizations. For mechanical stability, the proposed technology is suitable for a wide range of pressure forces. In particular, we proposed a highsensitivity sensor that allows the measuring of pressure forces corresponding to weights of 5 g and can be easily implemented in tactile robotic systems including shape and dielectric permittivity sensing. According to robotic systems, the mechanical control system, the signal processing, and the analysis of some important aspects such as sheer force detection, angle of incidence, sensitivity, electronics, and signal saturation represent the final goal of our work. The implementation of the proposed robotic system, including the shape detection algorithm, is also in progress.

The sensor is designed and optimized by means of experimental optical and preliminary mechanical characterizations.

References

[1] S. M. Firdaus, I. A. Azid, O. Sidek, K. Ibrahim, and M. Hussien, "Enhancing the resistivity of a mass-based piezoresistive micro-electromechanical systems cantilever sensor," *Micro Nano Lett*., vol. 5, no. 2, pp. 85–90, 2010.

[2] B. J. Kane,M. R. Cutkosaky, and T. A. Kovacs, "A traction stress sensor array for use in high resolution robotic tactile image," J. *Microelectromech. Syst*., vol. 9, no. 4, pp. 425–434, 2000.

[3] D. J. Beebe, A. S. Hseih, D. D. Denton, and R. G. Radwin, "A silicon force sensor for robotics and medicine," *Sens. Actuator A*, vol. 50, no. 1-2, pp. 55–56, 1995.

[4] J. I. Lee, X. Huang, and P. B. Chu, "Nanoprecision MEMS capacitive sensor for linear and rotational positioning," *IEEE* J. *Microelectromech. Syst*., vol. 18, no. 3, pp. 660–670, 2009.

[5] B. L. Gray and R. S. Fearing, "A surface micromachined micro tactile sensor array," in *Proc. IEEE Int. Conf. Robotics and Automation*, 1996, pp. 1–6.

[6] M. Leineweber, G. Pelz, M. Schmoidt, H. Kappert, and G. Zimmer, "New tactile sensor chip with silicone rubber cover," *Sens. Actuator A*, vol. 84, no. 84, pp. 236–245, 2000.

[7] C. Li, P. M. Wu, L. A. Shutter, and R. K. Narayan, "Dual-mode operation of flexible piezoelectric polymer diaphragm for intracranial pressure measurement," *App. Lett*., vol. 96, no. 5, pp. 053502–053502-3, 2010.

[8] E. S. Kolesar and C. S. Dyson, "Object image with a piezoelectric robotic tactile sensor," J. *Microelectromech. Syst*., vol. 4, no. 2, pp. 87–96, 1995.

[9] R. R. Reston and E. S. Kolesar, "Robotic tactile sensor array fabricated from a piezoelectric polyvinylidine fluoride film," in *Proc. IEEE NAECON*, 1990, pp. 1139–1144.

[10] H. S. Ko, C. W. Liu, and C. Gau, "Novel fabrication of a pressure sensor with polymer material and evaluation of its performance," J. *Micromech. Microeng*., vol. 17, no. 8, pp. 1640–1648, 2007.

[11] J. Martin, W. Bacher, O. F. Hagena, and W. K. Schomburg, "Strain gauge pressure and volume-flow transducers made by thermoplastic molding and membrane transfer," in *Proc. MEMS* 1998, pp. 361–366.

[12] A. V. Shirinov and W. K. Schomburg, "Polymer pressure sensor from PVDF," in *Proc. 20th Eurosensors*, 2006, vol. 1, pp. 84–85.

[13] K. Arshak, D. Morris, A. Arshak, O. Korostysnska, E. Jafer, D. Waldron, and J. Harris, "Development of polymer-based sensors for integration into a wireless data acquisition system suitable for monitoring environmental and physiological processes," *Biomol. Eng*., vol. 23, no. 5, pp. 253–257, 2006.

[14] H. S. Ko and C. Gau, "Bonding of a complicated polymer microchannel system for study of pressurized liquid flow characteristics with the electric double effect," *J. Micromech. Microeng*., vol. 19, no. 11, pp. 1–13, 2009.

[15] J. S. Heo, J. H. Chung, and J. J. Lee, "Tactile sensor array using fiber Bragg grating sensors," *Sens. Actuator A*, vol. 126, no. 2, pp. 312–327, 2006.

[16] S. Saga, H. Kajimoto, and S. Tachi, "High-resolution tactile sensor using the deformation of a reflection image," *Sensor Rev*., vol. 27, no. 1, pp. 35–42, 2007.

[17] Y. Yamada, Y. Iwanaga, M. Fukunaga, N. Fujimoto, E. Ohta, T. Morizono, and T. Umetani, "Soft viscoelastic robot skin capable of accurately sensing contact location of object," in *Proc. IEEE/SICE/RSJ Int. Conf. Multisensor Fusion and Integration for Intelligent Systems, MFI*, 1999, pp. 105–110.

[18] Y. Yamada, T. Morizono, Y. Umetani, and H. Takahashi, "Highly soft viscoelastic robot skin with a contact object-location-sensing capability," *IEEE Trans. Ind. Electron*., vol. 52, no. 4, pp. 960–968, 2005.

[19] Y. Ohmura, Y. Kuniyoshi, and A. Nagakubo, "Conformable and scalable tactile sensor skin for curved surfaces," in *Proc. Int. Conf. Robotics and Automation, ICRA*, 2006, pp. 1348–1353.

[20] J. Rebman and K. A. Morris, "A tactile sensor with electrooptical transduction," in *Robot Sensors*, vol. 2, Tactile and Non-Vision, A. Pugh, Ed. New York: Springer-Verlag, 1986, pp. 145–155.

[21] B. M. Cowie, D. J. Webb, B. Tam, P. Slack, and P. N. Brett, "Fibre Bragg grating sensors for distributive tactile sensing," *Meas. Sci. Technol*., vol. 18, no. 1, pp. 138–146, 2007.

[22] B. M. Cowie, D. J. Webb, B. Tam, P. Slack, and P. N. Brett, "Distributive tactile sensing using fibre Bragg grating sensors for biomedical applications," in *Proc. IEEE/RAS-EMBS Int. Conf. Biomedical Robotics and Biomechatronics, BioRob* 2006, pp. 312–317.

[23] P. Yong-Lae, K. Kau, R. J. Black, and M. R. Cutkosky, "Force sensing robot fingers using embedded fiber Bragg grating sensors and shape deposition manufacturing," in *Proc. Int. Conf. Robotics and Automation*, 2007, pp. 1510–1516.

[24] Q. Zhang, J. J. Xu, Y. Liu, and H. Y. Cuen, "In-situ synthesis of poly (dimethylsiloxane)-gold nanoparticles composite films and its application in microfluidic system," *Lab Chip*, 2008, vol. 8, pp. 352–357.

[25] C. E. Hoppe, C. Ridriguez-Abreu, M. Lazzari, M. A. Lopez-Quintela, and C. Solans, "One-pot preparation of gold-elastomer nanocomposites using PDMS-graft-PEO copolymer micelles as nanoreactors," *Phys. Stat. Sol. A*, vol. 205, no. 6, pp. 1455–1459, 2008.

[26] A. Massaro, F. Spano, P. Cazzato, R. Cingolani, and A. Athanassiou, "Real time optical pressure sensing for tactile detection using gold nanocomposite material," in *Proc. MNE* 2010, pp. 121–122.

[27] A. Rakic, A. B. Djurisic, J. M. Elazar, and M. L. Majewski, "Optical properties of metallic films for vertical-cavity optoelectronic devices," *Appl. Opt*., vol. 37, no. 22, pp. 5271–5283, 1998.

[28] M. Chen and R. G. Horn, "Refractive index of sparse layers of absorbed gold nanoparticles," *J. Coll. Interface Sci*., vol. 315, no. 2, pp. 814–817, 2007.

[29] A.Massaro, V. Errico, T. Stomeo, A. Salhi, R. Cingolani, A. Passaseo, and M. De Vittorio, "3D FEMmodeling and fabrication of circular photonic crystalmicrocavity," *IEEE J. Light Technol*., vol. 26,no. 16, pp. 2960–2968, 2008.

Alessandro Massaro, Italian Institute of Technology IIT, Center for Biomolecular Nanotechnologies of Arnesano (LE), Italy. E-mail: alessandro.massaro@iit.it.

Fabrizio Spano, Italian Institute of Technology IIT, Center for Biomolecular Nanotechnologies of Arnesano (LE), Italy. E-mail: Fabrizio.spano@iit.it.

Paolo Cazzato, National Nanotechnology Laboratory, Institute of Nanoscience of CNR of Lecce, Italy. E-mail: paolo.cazzato@nano.cnr.it.

Carola La Tegola, National Nanotechnology Laboratory, Institute of Nanoscience of CNR of Lecce, Italy. E-mail: carola.lategola@nano.cnr.it.

Roberto Cingolani, Italian Institute of Technology IIT of Genova, Italy. E-mail: roberto.cingolani@iit.it.

Athanassia Athanassiou, Italian Institute of Technology IIT, Center for Biomolecular Nanotechnologies of Arnesano (LE), Italy. E-mail: athanassia.athanassiou@iit.it.